Effect of Nb addition on the glass forming ability and mechanical properties in the Ni-Zr-Al-Hf-Nb alloys

W. B. KIM, B. J. YE, S. YI*
Department of Materials Science and Metallurgy, Kyungpook National University, 1370 Sankyuk-dong, Buk-gu, Daegu 702-701, Korea
E-mail: yish@knu.ac.kr

Published online: 10 April 2006

The effect of substituting Nb for Zr on the glass forming ability (GFA) and mechanical properties of $Ni_{60}Zr_{27-x}Al_6Hf_7Nb_x$ ($x = 0 - 14$) alloys was investigated. The substitution of Zr with Nb of 0 – 14 at% improved the GFA. When increasing the Nb content x from 0 – 14, the glass transition temperature, T_g, and the crystallization temperature, T_x, of melt-spun $Ni_{60}Zr_{27-x}Al_6Hf_7Nb_x$ ($x = 0 - 14$) alloys increased from 833 and 863 K to 877 and 914 K, respectively. The $Ni_{60}Zr_{27-x}Al_6Hf_7Nb_x$ ($x = 8$, 10, 12 and 14) alloys exhibited high $T_{rg} (= T_g/T_m^{liq})$ (>0.615), $\gamma (= T_x/T_g + T_m^{liq})$(>0.4) values and a wide supercooled liquid region, $\Delta T_x (= T_x - T_g)$ (>36 K) enabling the fabrication of bulk metallic glass (BMG) with a diameter above 1 mm. As such, $Ni_{60}Zr_{17}Al_6Hf_7Nb_{10}$ and $Ni_{60}Zr_{15}Al_6Hf_7Nb_{12}$ alloys with a maximum diameter of 2 mm could be fabricated by injection casting. These bulk amorphous alloys also exhibited good mechanical properties, where the true ultimate compressive strength, strain and Vickers hardness (H_v) were approximately 3.0 GPa, 2.08% and 713, respectively, for the amorphous $Ni_{60}Zr_{17}Al_6Hf_7Nb_{10}$ alloy, and 3.1 GPa, 2.22% and 687, respectively, for the amorphous $Ni_{60}Zr_{15}Al_6Hf_7Nb_{12}$ alloy.

1. Introduction

Bulk metallic glasses (BMGs) and amorphous alloys are of interest because of their unique properties, such as high strength, corrosion resistance and magnetic properties, associated with random atomic configurations [1]. More recently, BMGs alloys with a high glass forming ability (GFA) have been developed mainly in Zr-, Ti-, Cu-, Mg- and Fe-based alloy systems [2–7]. Meanwhile, the development of Ni-based amorphous alloys with high strength and corrosion resistance has dominated the practical application of amorphous alloys. Although quite a few high-strength glass-forming systems [2, 8, 9] have been reported, the GFA achieved so far has been very limited. Also, some of these reported systems [2] include metalloids, such as B and P, in their chemical compositions, which limits the manufacturability of these alloys. Thus, for broader engineering applications and scientific studies on Ni-based BMGs, new Ni-based alloys are needed with a higher GFA and better manufacturability. Recently, Ni-Zr-Al-based bulk amorphous alloys (containing more than 60 at% Ni) with a large supercooled liquid region, ΔT_x, high reduced glass transition temperature, T_{rg}, and γ have been reported through a systematic alloy design [8, 10, 11].

Accordingly, the present study examined the effect of Nb, as an element substituting for Zr, on the GFA and mechanical properties of $Ni_{60}Zr_{27-x}Al_6Hf_7Nb_x$ ($x = 0$, 4, 6, 8, 10, 12 and 14) alloys. Nb was selected as a candidate element based on the empirical rules for a high GFA [12], i.e., Nb has an intermediate atomic radius (Ni < Al < Nb < Zr < Hf) [13] and produces a significant amount of heat when mixing the constituting elements [14]. Thus, to study the effect of Nb as a substituting element for Zr on the GFA and mechanical properties of $Ni_{60}Zr_{27-x}Al_6Hf_7Nb_x$ alloys, the variation in the glass transition temperature (T_g), crystallization temperature (T_x) and melting temperature (T_m^{liq}) according to the Nb content was investigated by a thermal analysis of melt spun amorphous $Ni_{60}Zr_{27-x}Al_6Hf_7Nb_x$ ($x = 0$, 4, 6, 8, 10, 12 and 14) alloys. Thereafter, to examine the glass forming ability, bulk glassy samples were prepared using the injection casting method. Finally, the mechanical

*Author to whom all correspondence should be addressed.
0022-2461
DOI: 10.1007/s10853-006-2228-4

properties were considered base on compressive and hardness tests.

2. Experimental

Alloys of nominal composition (at%) $Ni_{60}Zr_{27-x}Al_6Hf_7Nb_x$ (x = 0, 4, 6, 8, 10, 12 and 14) were prepared by arc-melting under Ar atmosphere. Raw materials with a purity ranging from 99.8 to 99.99% were used in the arc-melting process. The alloys were remelted at least four times to ensure their compositional homogeneity. Rapidly solidified ribbon samples were prepared by remelting the alloys in quartz tubes, and ejecting with an over pressure of 35 kPa through a nozzle onto a Cu wheel rotating with a surface velocity of 40 m/s. The resulting ribbons exhibited a thickness of about 25 – 30 μm and width of about 2 mm. Rod-shaped bulk samples were prepared using an injection casting with a diameter of 1 and 2 mm and height of about 50 mm. X-ray diffraction (XRD) experiments were performed to identify the formation of the amorphous phase in the ribbons and bulk samples using monochromatic Cu K_α radiation. A thermal analysis of the ribbon samples was carried out to determine the glass transition temperature and crystallization temperature using differential scanning calorimetry (DSC) during continuous heating at a heating rate of 0.67 K/s. In addition, a differential thermal analysis (DTA) was performed to measure the temperature range of the alloy melting endotherms during continuous heating at a heating rate of 0.33 K/s. From the cast rods, cylindrical specimens with dimension of $\phi 1 \times 2.3$ mm were prepared and an uniaxial compression test conducted under the conditions of a constant cross-head speed (Initial strain rate = 1×10^{-4} s^{-1}) at room temperature on an Instron-type machine. Also, micro hardness was performed using Vickers microhardness tester under a load of 200 gf.

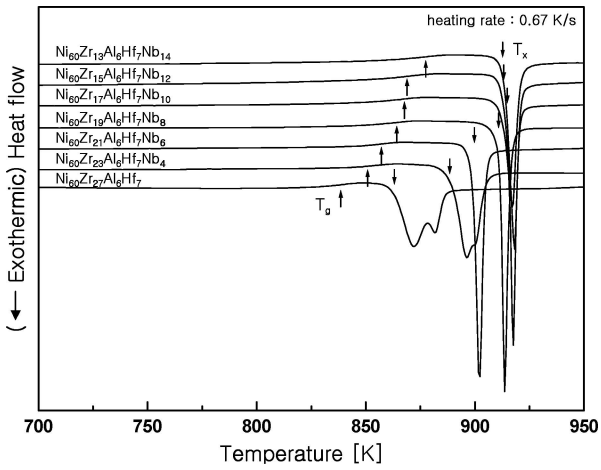

Figure 1 DSC traces obtained from the melt-spun $Ni_{60}Zr_{27-x}Al_6Hf_7Nb_x$ ($x = 0 - 14$) amorphous ribbons during continuous heating at a heating rate of 0.67 K/s.

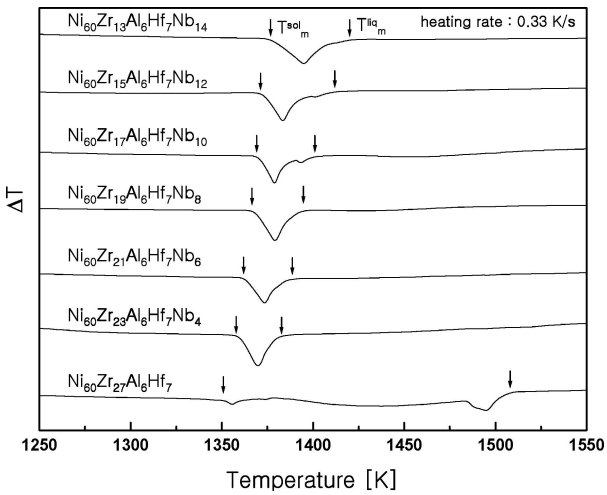

Figure 2 DTA traces obtained from the melt-spun $Ni_{60}Zr_{27-x}Al_6Hf_7Nb_x$ ($x = 0 - 14$) amorphous ribbons during continuous heating at a heating rate of 0.33 K/s.

3. Results

3.1. Thermal analysis

The formation of the amorphous phase was confirmed by XRD experiments in all the rapidly solidified $Ni_{60}Zr_{27-x}Al_6Hf_7Nb_x$ (x = 0 – 14) alloy ribbons. Fig. 1 shows the DSC traces obtained from the melt-spun $Ni_{60}Zr_{27-x}Al_6Hf_7Nb_x$ (x = 0 – 14) alloy ribbons during continuous heating at a rate of 0.67 K/s. All the traces showed an endothermic event, which is characteristic of glass transition, followed by several exothermic peaks corresponding to crystallization into glass. With an increasing Nb content, the glass transition temperature (T_g) and the onset temperature of the first crystallization temperature (T_x) increased from 838 K and 863 K at $x = 0$ to 877 K and 913 K at $x = 14$, respectively. The supercooled liquid region (ΔT_x) increased from 24 K at $x = 0$ to 47 K at $x = 8$, 10, and then decreased with a further increase of x, reaching 36 K at $x = 14$. In addition, the two overlapped exothermic peaks at $x = 0$ and 4 changed to a single exothermic peak at x = 6, 8, 10, 12 and 14, indicating a change in the crystallization behavior.

Fig. 2 shows the DTA traces obtained from the melt-spun $Ni_{60}Zr_{27-x}Al_6Hf_7Nb_x$ (x = 0 – 14) alloy ribbons during continuous heating at a rate of 0.33 K/s. The solidus temperature (T_m^{sol}) and liquidus temperature (T_m^{liq}) assumed to be the onset and end temperature, respectively, of the melting endotherm. The $Ni_{60}Zr_{27}Al_6Hf_7$ alloy exhibited two endothermic peaks with onset and end temperatures of 1350 and 1508 K, respectively. The T_m^{sol} and T_m^{liq} for the alloys exhibited a dependence on the Nb contents (x). The alloy with $x = 0$ showed minimum T_m^{sol} at about 1350 K, while the other alloys exhibited T_m^{sol} within a range of 1358 – 1376 K. As such, there was no significant change in T_m^{sol} with the Nb content x. However, the T_m^{liq} changed with a large adding of Nb, i.e. T_m^{liq} was 1508 K at $x = 0$, decreasing to 1382 K at $x = 4$, then slightly increased to 1419 K at $x = 14$. The detailed results of the DSC and DTA traces are summarized in Table I.

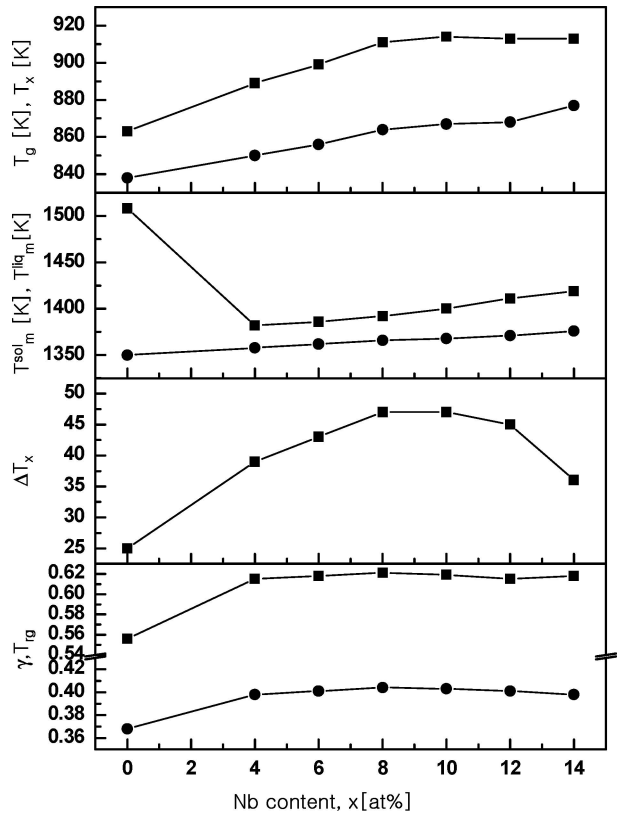

Figure 3 Variations of T_x, T_g, T_m^{liq}, T_m^{sol}, ΔT_x, T_{rg} and γ obtained from the melt-spun $Ni_{60}Zr_{27-x}Al_6Hf_7Nb_x$ ($x = 0, 4, 6, 8, 10, 12, 14$) amorphous ribbons.

Fig. 3 shows the variation of T_x, T_g, T_m^{sol}, T_m^{liq}, ΔT_x, T_{rg} and γ for melt-spun $Ni_{60}Zr_{27-x}Al_6Hf_7Nb_x$ ($x = 0$ – 14) alloys. The supercooled liquid range, ΔT_x ($= T_x - T_g$) increased from 25 K at $x = 0$ to 47 K at $x = 8$ and 10, then decreased with a further increase of x, reaching 36 K at x =14. To obtain a glass transition during solidification, the nucleation and growth of a competing crystalline phase should be prevented in the temperature range between T_m^{liq} and T_g. Therefore, a large difference between T_m^{liq} and T_g does not favor the glass formation. This difference can be presented by using a reduced glass transition temperature, $T_{rg}(= T_g/T_m^{liq})$. With increasing x, the T_{rg} increased from 0.556 at $x = 0$ to 0.621 at $x = 8$, then decreased with a further increase of x, reaching 0. 618 at $x = 14$. However, when increasing x, the $\gamma(= T_x/= T_x(T_g + T_m^{liq}))$ increased from 0.368 at $x = 0$ to 0.403 at $x = 10$, then decreased with a further increase of x, reaching 0. 398 at $x = 14$.

3.2. Bulk glass formation

To examine the improvement of the glass forming ability of each alloy composition, the $Ni_{60}Zr_{27-x}Al_6Hf_7Nb_x$ ($x =$ 0 – 14) alloys were injection cast into cylindrical cavities of Cu molds with the diameters of 1 and 2 mm. The maximum diameters for amorphous phase formation of the alloys are summarized in Table I. The $Ni_{60}Zr_{17}Al_6Hf_7Nb_{10}$ and $Ni_{60}Zr_{15}Al_6Hf_7Nb_{12}$ alloys showed a maximum diameter of 2 mm for fully amorphous phase formation. Fig. 4a and b show DSC traces obtained from the injection cast bulk $Ni_{60}Zr_{17}Al_6Hf_7Nb_{10}$ and $Ni_{60}Zr_{15}Al_6Hf_7Nb_{12}$ cylinders, together with the data from the melt-spun ribbon. The DSC trace from the injection cast bulk $Ni_{60}Zr_{17}Al_6Hf_7Nb_{10}$ and $Ni_{60}Zr_{15}Al_6Hf_7Nb_{12}$ cylinder with diameter 2 mm showed nearly same crystallization behavior as the ribbon sample with T_g and T_x, respectively. The integrated heat of the exotherms for the bulk sample was similar, including the experimental error, to that for the ribbon sample, indicating a fully amorphous structure in the injection cast sample.

Figs 5a and b show XRD patterns taken from the injection cast bulk $Ni_{60}Zr_{17}Al_6Hf_7Nb_{10}$ and $Ni_{60}Zr_{15}Al_6Hf_7Nb_{12}$ amorphous cylinders when $d =$ 1 and 2 mm, respectively. For comparison, the results from the melt-spun $Ni_{60}Zr_{17}Al_6Hf_7Nb_{10}$ and $Ni_{60}Zr_{15}Al_{6}Hf_7Nb_{12}$ ribbons are also included. All of the XRD patterns for the $Ni_{60}Zr_{17}Al_6Hf_7Nb_{10}$ and $Ni_{60}Zr_{15}Al_6Hf_7Nb_{12}$ alloys showed typical halo patterns.

3.3. Mechanical properties

An uniaxial compression test was conducted on the two bulk amorphous $Ni_{60}Zr_{17}Al_6Hf_7Nb_{10}$ and $Ni_{60}Zr_{15}Al_6Hf_7Nb_{12}$ cylinders with a diameter of 1 mm. Fig. 6 shows the uniaxial compressive true stress-strain curves for both alloys deformed under a constant crosshead speed condition (Initial strain rate $= 1 \times 10^{-4}$ s^{-1}) at room temperature. Both alloys exhibited a linear elastic behavior up to yielding, then maintain an almost constant stress level during plastic deformation. The true ultimate compressive strength and strain were approx-

TABLE I Nominal compositions of the investigated alloys and thermal properties (T_g, T_x, ΔT_x, T_m^{sol}, T_m^{liq}, T_{rg} and γ) obtained from the DSC and DTA continuous heating traces

Alloy	T_g (K)	T_x (K)	ΔT_x (K)	$T^{sol}{}_m$ (K)	$T^{liq}{}_m$ (K)	T_{rg}	γ	D_{max} (mm)
$Ni_{60}Zr_{27}Al_6Hf_7$	838	863	25	1350	1508	0.556	0.368	–
$Ni_{60}Zr_{23}Al_6Hf_7Nb_4$	850	889	39	1358	1382	0.615	0.398	–
$Ni_{60}Zr_{21}Al_6Hf_7Nb_6$	856	899	43	1362	1386	0.618	0.401	–
$Ni_{60}Zr_{19}Al_6Hf_7Nb_8$	864	911	47	1366	1392	0.621	0.404	1
$Ni_{60}Zr_{17}Al_6Hf_7Nb_{10}$	867	914	47	1368	1400	0.619	0.403	2
$Ni_{60}Zr_{15}Al_6Hf_7Nb_{12}$	868	913	45	1371	1411	0.615	0.401	2
$Ni_{60}Zr_{13}Al_6Hf_7Nb_{14}$	877	913	36	1376	1419	0.618	0.398	1

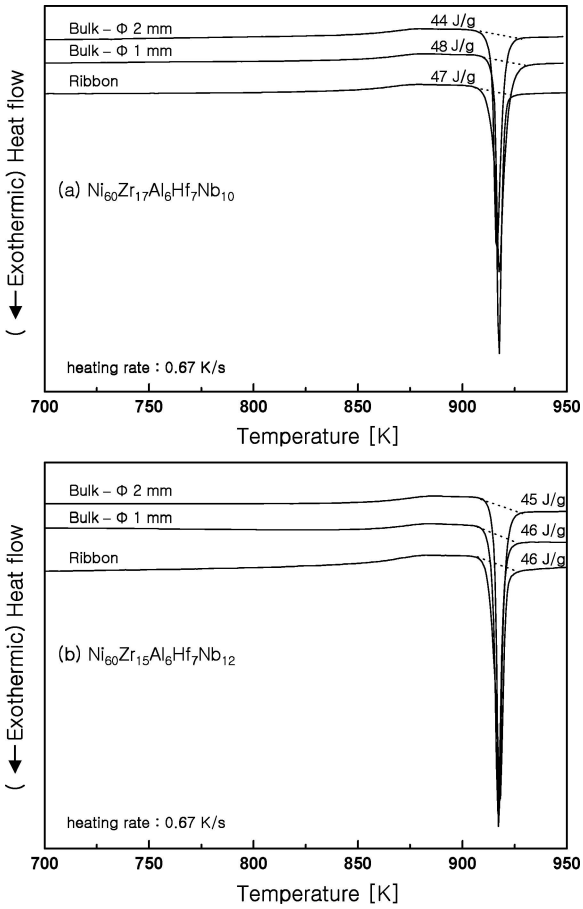

Figure 4 DSC traces obtained from the melt-spun ribbon and injection cast cylinders with 1 and 2 mm diameters, respectively, during continuous heating rate at a rate of 0.67 K/s: (a) $Ni_{60}Zr_{17}Al_6Hf_7Nb_{10}$ and (b) $Ni_{60}Zr_{15}Al_6Hf_7Nb_{12}$ alloys.

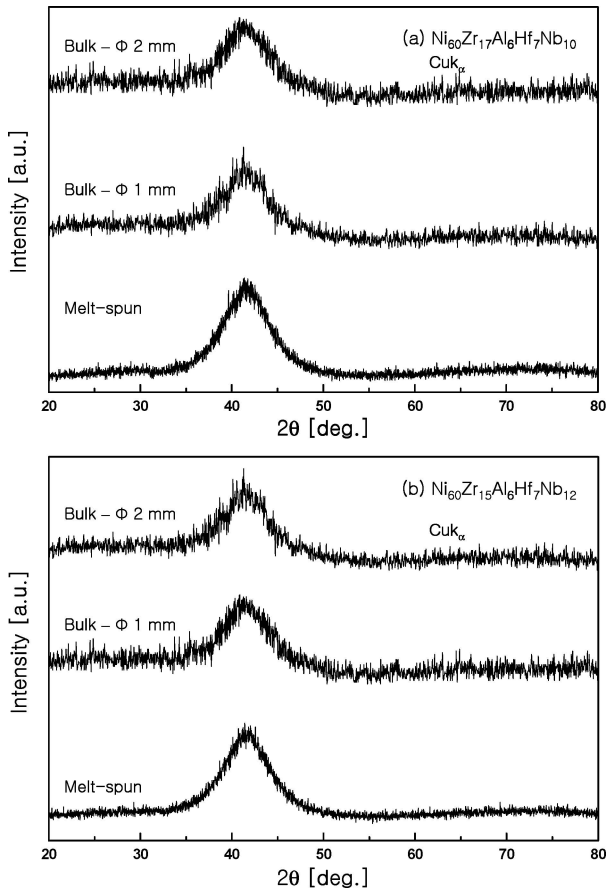

Figure 5 XRD patterns taken from the injection cast bulk $Ni_{60}Zr_{17}Al_6Hf_7Nb_{10}$ and $Ni_{60}Zr_{15}Al_6Hf_7Nb_{12}$ amorphous cylinders with $d = 1$ and 2 mm, respectively: (a) $Ni_{60}Zr_{17}Al_6Hf_7Nb_{10}$ and (b) $Ni_{60}Zr_{15}Al_6Hf_7Nb_{12}$ alloys. For comparison, the results from melt-spun ribbons are also included.

imately 3.0 GPa and 2.08%, respectively, for the amorphous $Ni_{60}Zr_{17}Al_6Hf_7Nb_{10}$ alloy, and 3.1 GPa and 2.22%, respectively, for the amorphous $Ni_{60}Zr_{15}Al_6Hf_7Nb_{12}$ alloy. Meanwhile, the Vickers hardness (H_v) was 713 for the amorphous $Ni_{60}Zr_{17}Al_6Hf_7Nb_{10}$ alloy and 687 for the amorphous $Ni_{60}Zr_{15}Al_6Hf_7Nb_{12}$ alloy.

4. Discussion

The effects of alloying elements on the GFA of an alloy have not been yet fully understood. However, the multicomponent interactions, as pointed out in the empirical rules [1], and thermal stability of the amorphous phase would appear to be related to the GFA of an alloy. The present study showed that addition of Nb to an Ni–Zr–Al-Hf alloy improved the thermal stability of the glassy phase, as clearly shown in Fig. 1. Moreover, the resistance of the liquid alloy to crystallization improved significantly with the addition of Nb, resulting in the presence of the alloy composition range with a wide supercooled region (>40 K). Although ΔT_x, T_{rg} and γ are not directly related to the GFA of the alloy, most BMGs have ΔT_x, T_{rg} and γ larger than 40 K, 0.6 and 0.4, respectively, at a heating rate of 0.67 K/s [1].

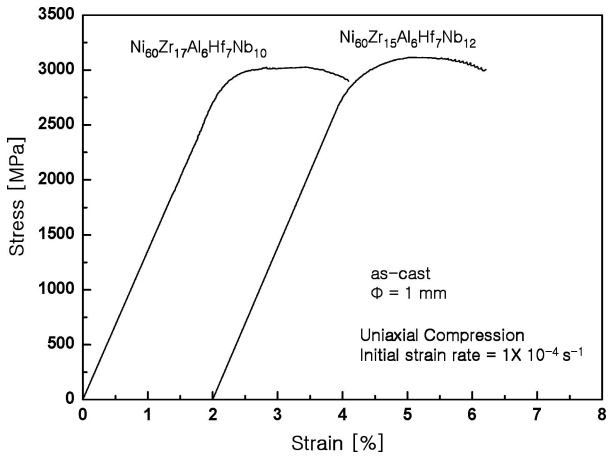

Figure 6 True compressive stress-strain curves of both $Ni_{60}Zr_{17}Al_6Hf_7Nb_{10}$ and $Ni_{60}Zr_{15}Al_6Hf_7Nb_{12}$ bulk amorphous alloys with a diameter of 1 mm.

The $Ni_{60}Zr_{27-x}Al_6Hf_7Nb_x$ ($x = 8$, 10, 12, 14) alloys exhibited a large ΔT_x (>36 K) and high T_{rg} (>0.615) and γ (>0.4) values, enabling the fabrication of BMG with a diameter above 1 mm. As such, $Ni_{60}Zr_{17}Al_6Hf_7Nb_{10}$ and $Ni_{60}Zr_{15}Al_6Hf_7Nb_{12}$ alloys with a maximum diameter of 2 mm could be fabricated by injection casting. It should

also be noted that the GFA of the Ni-Zr-Al-Hf-Nb alloys improved, when the addition of Nb decrease the melting temperature, while increasing the T_g and T_x.

A decrease in melting point and increase of T_g and T_x indicate that the liquid phase, including glass state, is stabilized with respect to competing crystalline phases. The liquid phase can be stabilized by increasing the atomic packing density and by forming short-range compositional order in the liquid phase [15]. As such, the large atomic size difference between Nb and constitution elements was favorable to increase the atomic packing density of the liquid structure. Plus, the strong interaction Ni-Nb (−30 kJ/mol) and Al-Nb (−18 kJ/mol) atomic pairs may also have contributed to stabilization of the liquid phase by change the local atomic structure [14].

5. Conclusion

The glass forming ability and mechanical properties of $Ni_{60}Zr_{27-x}Al_6Hf_7Nb_x$ (x = 0 – 14) alloys were investigated. The GFA improved when the addition of Nb decreased the melting temperature, while increasing the crystallization onset temperature and glass transition temperature. The substitution of Zr with Nb at 0 – 14 at% improved the GFA. When increasing the Nb content x from 0 – 14, the glass transition temperature and the crystallization temperature of melt-spun $Ni_{60}Zr_{27-x}Al_6Hf_7Nb_x$ ($x = 0 – 14$) alloys increased from 833 to 877 K, and 863 to 914 K, respectively. The supercooled liquid range also increased from 25 K at $x = 0$ to 47 K at $x = 8$ and 10, then decreased with further increase of x, reaching 36 K at $x = 14$. The $Ni_{60}Zr_{27-x}Al_6Hf_7Nb_x$ (x = 8, 10, 12, 14) alloys exhibited a large ΔT_x (>36 K) and high T_{rg} (>0.615) and γ (>0.4) values, enabling the fabrication of bulk metallic glass (BMG) with a diameter above 1 mm. As such, the amorphous $Ni_{60}Zr_{17}Al_6Hf_7Nb_{10}$ and $Ni_{60}Zr_{15}Al_6Hf_7Nb_{12}$ alloys achieved a maximum diameter of 2 mm due to their good GFA, as investigated in the present study. Both amorphous alloys prepared by melt spinning and injection casting showed similar crystallization process during continuous heating in the DSC. In addition, these bulk amorphous alloys also exhibited good mechanical properties, where the true ultimate compressive strength, strain and Vickers hardness (H_v) were approximately 3.0 GPa, 2.08% and 713, respectively, for the amorphous $Ni_{60}Zr_{17}Al_6Hf_7Nb_{10}$ alloy, and 3.1 GPa, 2.22% and 687, respectively, for the amorphous $Ni_{60}Zr_{15}Al_6Hf_7Nb_{12}$ alloy.

Acknowledgment

This work was financially supported by MOCIE (Ministry of Commerce, Industry and Energy) under the project named development of structural metallic materials and parts with super strength and high performance.

References

1. A. INOUE, *Acta Mater.* **48** (2000) 279.
2. X. WANG, I. YOSHII, A. INOUE, Y. H. KIM and I. B. KIM, *Mater. Trans. JIM* **40** (1999) 1130.
3. J. M. PARK, Y. C. KIM, W. T. KIM and D. H. KIM, *J. Mater. Res.* **19** (2004) 2221.
4. D. XU, G. DUAN and W. L. JOHNSON, *Phys. Rev. Lett.* **92** (2004) 245504.
5. E. S. PARK, H. G. KANG, W. T. KIM and D. H. KIM, *J. Non-Cryst. Solids* **279** (2001) 154.
6. V. PONNAMBALAM, S. J. POON, G. J. SHIFLET, V. M. KEPPENS, R. TAYLOR and G. PETCULESCU, *Appl. Phys. Lett.* **83** (2003) 1131.
7. J. -H. KIM, J. S. PARK, E. FLEURY, W. T. KIM and D. H. KIM, *Mater. Trans.* **45** (2004) 2770.
8. S. YI, J. S. JANG, W. T. KIM and D. H. KIM, *Mater. Lett.* **48** (2001) 258.
9. H. C. YIM, D. H. XU and W. L. JOHNSON, *Appl. Phys. Lett.* **82** (2003) 1030.
10. J. H. NA, W. T. KIM, D. H. KIM and S. YI, *Mater. Lett.* **58** (2004) 778.
11. W. B. KIM, B. J. YE and S. YI, *Met. Mater. Int.* **10** (2004) 1.
12. A. INOUE, A. TAKEUCHI and T. ZHANG, *Metall. Mater. Trans.* **29A** (1998) 1779.
13. C. J. SMITHELLS and E. A. BRANDES, in "Metals Reference Book", 5th edn. (Butterworths, London, 1976).
14. F. R. BOER, R. BOOM, W. C. M. MATTERNS, A. R. MIEDEMA and A. K. NIESSEN, in "Cohesion in Metals" (Noth-Holland, Amsterdam, 1988).
15. E. S. PARK, H. K. LIM, W. T. KIM and D. H. KIM, *J. Non-Cryst. Solids.* **298** (2002) 15.

Received 17 November 2004
and accepted 13 May 2005